Modeling of Flatness-Based Control with Disturbance Observer-Based Parameter Estimation for PMSM Drive

S. Sriprang*[1,2,3], B. Nahid-Mobarakeh[1], N. Takorabet[1], P. Thounthong[2,3], S. Pierfederici[6], P. Kumam[4], N. Bizon[5] and P. Mungporn[2]

[1]GREEN Lab., Université de Lorraine, 2 Vancouver-les-Nancy, Lorraine 54516, France

[2]Renewable Energy Research Centre (RERC), Thai-French Innovation Institute (TFII)

[3]Department of Teacher Training in Electrical Engineering (TE), Faculty of Technical Education King Mongkut's University of Technology North Bangkok, 1518, Pracharat 1 Rd., Bangkok 10800, Thailand

* Corresponding author: songklod.sriprang@univ-lorraine.fr, songklod.sri@rmutr.ac.th

[4]Department of Mathematics, King Mongkut's University of Technology Thonburi, Bangkok, Thailand

[5]Faculty of Electronics, Communications and Computers, University of Pitesti, Arges 110040, Pitesti, Romania

[6]LEMTA Lab., Université de Lorraine, 2 Vancouver-les-Nancy, Lorraine 54516, France

Abstract: - This paper presents a modeling of nonlinear control with parameters identification for the permanent magnet synchronous motor (PMSM) drive. A resistance in series with an inductance and the conduction losses in semiconductor switching devices of inverters represented by v_{tq} ($=R_s*i_q$) as well as the torque load T_L are going to be estimated by observer method based on extended Luenberger observer (LOB). The simulation and experimental results show the proposed control provides the rapid response and flat of the current control loop for the PMSM drive system. Moreover, the observer approach precisely estimates both v_{tq} and T_L, and the converging time is less than 0.1 sec. The test bench was implemented by small-scale PMSM 1 kW, 3,500 rpm, 6 ampere rated to validate the proposed control approach.

Key-Words: - Disturbance observer (DOB), SPMSM, Flatness-based control modeling, Extended Luenberger Observer

Received: August 1, 2018. Revised: September 10, 2018. Accepted: October 2, 2018. Published: October 9, 2018.

1 Introduction

Currently, Permanent-Magnet Synchronous Machines (PMSMs) have been widely used in many applications such as robotics, numerical controls, and electric vehicles, etc., since they have the significant advantages like high power ratio, small volume, and simple structure. Moreover, with the development of a full electric aircraft, PMSMs are the appropriate player for the electrical propulsion system in aviation. Although there are many advantages of PMSMs, it is still challenging to control them getting high performance for all operating conditions. It is due to a nonlinear multivariable system and subjected to unknown parameters uncertainty of them that nonlinear control approaches are more reasonable than linear control. To get around this problem, many researchers have proposed diverse control design methods, e.g., adaptive control [1], neural network control [2], nonlinear feedback linearization control [3], disturbance-observer-based control [4], model predictive control [5], fuzzy-logic-based controller [6], robust control [7] and the combination of these concepts [8]. One of the nonlinear control systems adapted to control PMSM is the flatness-based control system [9]-[10]. As the flatness-based control is a model-based control, the performance of the controller relies on the accuracy of the machine parameters such as the stator resistance R_s, load torque disturbance T_L, etc. However, these are difficult to measure directly, so state observer method is often utilized to estimate these parameters. Many parameter estimation methods have been investigated in the literature review, and one of the observer methods is Extended Luenberger Observer (ELO) that has advantages over conventional observers such as independence from mathematical model accuracy, robustness, and good dynamic performance [11]. Also, only observer gains need to be tuned, and the tuning process is not complicated because the gains are determined by the desired observer. In this paper, flatness-based control is going to utilize to control PMSM, and also an observer approach is introduced to improve the performance of the proposed control. In the following sections, a detailed theoretical analysis of the proposed method is presented. Finally, practical implementation results based on the dSPACE 1104 DSP system are shown to confirm its correctness.

2 Proposed Control Design

2.1 Modeling of the PMSM/inverter

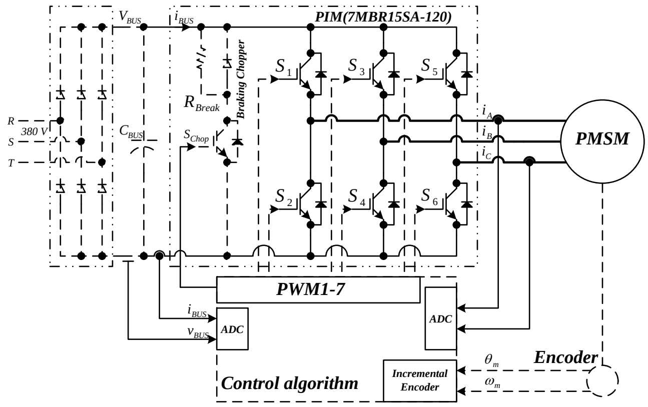

Fig. 1 A three-phase inverter is driving the PMSM where V_{BUS}, i_{BUS}, i_A, and i_C are DC bus voltage, the input inverter current, the motor phase current, respectively.

Fig. 1 shows a system configuration of a three-phase inverter connected to the PMSM. The sinusoidal pulse-width modulation technique (SPWM) is applied to inverter to achieve a sinusoidal output voltage with minimal undesired harmonics. The classic rotor reference frame of the PMSM is [9]-[12]:

$$\frac{di_d}{dt} = \frac{1}{L_d}(v_d - R_s \cdot i_d + \omega_e \cdot L_q \cdot i_q) \tag{1}$$

$$\frac{di_q}{dt} = \frac{1}{L_q}(v_q - R_s \cdot i_q - \omega_e \cdot L_d \cdot i_d - \omega_e \cdot \psi_m) \tag{2}$$

$$\frac{d\omega_m}{dt} = \frac{1}{J}(T_e - B \cdot \omega_m - T_L) \tag{3}$$

Where

$$T_e = p \cdot i_q \cdot (\Psi_m - (L_q - L_d) \cdot i_d) \tag{4}$$

$$\omega_e = p \cdot \omega_m \tag{5}$$

v_d and v_q are the d, q axis voltages, i_d and i_q are the d, q axis stator currents, L_d and L_q are the d, q axis inductances, R_s and Ψ_m are the resistance (or system losses) and the magnet's flux linkage, respectively; and ω_e, ω_m, p, T_e, T_L, B, J are electrical angular frequency, mechanical angular frequency, number of pole pairs, electromagnetic torque, load torque, viscosity, and inertia, respectively.

2.2 Flatness-based Control design

For the first is to analyze the flatness-based control that is mentioned by [9], to utilize for PMSM control. As $L_s = L_q = L_d$ is defined for non-salient machine. Flat outputs $y = [i_d \ i_q \ \omega_m]^T$, control variable $u = [v_d \ v_q \ i_q]^T$, and state variable $x = [i_d \ i_q \ \omega_m]^T$ are assigned respectively. Then, the state variables x can be written as $x = [\varphi_1(y_1) \ \varphi_2(y_2) \ \varphi_3(y_3)]^T$. From (1), (2), and (3), the control variable u can be calculated from the flatness output y and its time derivatives (*called inverse dynamics*):

$$u_1 = L_s \cdot \dot{i}_d + R_s \cdot i_d - \omega_e \cdot L_s \cdot i_q = \psi_1(y_1, \dot{y}_1, y_2) = v_d \tag{6}$$

$$u_2 = L_s \cdot \dot{i}_q + R_s \cdot i_q + \omega_e \cdot L_s \cdot i_d + \omega_e \cdot \Psi_m = \psi_2(y_1, y_2, \dot{y}_2) = v_q \tag{7}$$

$$u_3 = (J \cdot \dot{\omega}_m + T_L + B_f \cdot \omega_m) / p \cdot \Psi_m = \psi_3(y_3, \dot{y}_3) = i_{qCOM} \tag{8}$$

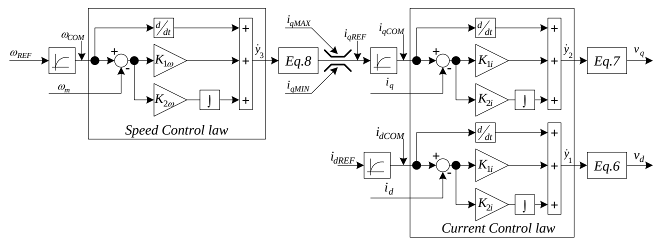

Fig. 2 Flatness-based control block diagram.

The control law of the current and speed control loop detailed depicts in Fig. 2. The input reference of each module of the current control is y_{iREF}, where i = 1, 2, ($y_{1REF} = i_d = 0$, and $y_{2REF} = i_{qCOM}$), and the input reference of the speed control is $y_{3REF} = \omega_{COM}$. The control law based on the second-order control law is used by (9) for current loop and (10) for the speed loop, to guarantee that the control of the flatness output variable converges to their reference trajectory.

$$\dot{y}_i = \dot{y}_{iREF} + K_{1i}(y_{iREF} - y_i) + K_{2i}\int_0^t (y_{iREF} - y_i)d\tau \tag{9}$$

$$\dot{y}_3 = \dot{y}_{3REF} + K_{1\omega}(y_{3REF} - y_3) + K_{2\omega}\int_0^t (y_{3REF} - y_3)d\tau \tag{10}$$

where K_{1i}, K_{2i}, $K_{1\omega}$, and $K_{2\omega}$ are the controller parameters defining as follows:

$K_{1i} = 2\zeta_1\omega_1$, $K_{2i} = \omega_1^2$, $K_{1\omega} = 2\zeta_3\omega_3$, $K_{2\omega} = \omega_3^2$

Fig. 3 shows the whole control system of the PMSM control using the flatness-based control system proposed in this research. Error tracking ($e_1 = y_{iREF} - y_i$) and ($e_2 = y_{3REF} - y_3$) are defined as follows

$$q_i(s) = e_1^2 + 2\zeta_1\omega_1 e_1 + \omega_1^2 \tag{11}$$

$$q_\omega(s) = e_2^2 + 2\zeta_3\omega_3 e_2 + \omega_3^2 \tag{12}$$

ζ_1 and ζ_3, are the desired dominant damping ratio, and ω_1 and ω_3 are natural frequency respectively.

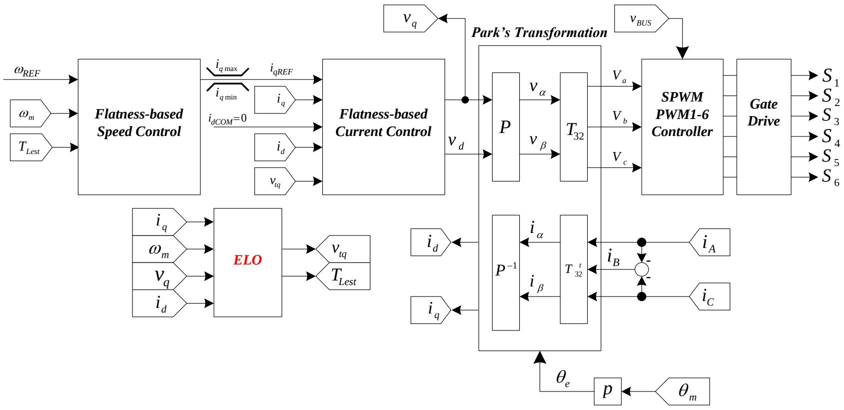

Fig. 3 Proposed control block diagram.

It is evident that the control system is stable for the positive value of K_{1i}, K_{2i}, $K_{1\omega}$, and $K_{2\omega}$. However, "*based on a cascade control structure and constant switching frequency in power electronic inverters, the frequencies of the system must meet the following rule: $\omega_3 << \omega_1 << \omega_s$, where ω_3 is the cut off frequency of the speed control loop, ω_1 is the cut off frequency of the current control loop and ω_s is the switching frequency*" [24]. Finally, a second-order is used by (13) to limit the transient current and speed command, so that they are going to keep smooth transition during the instantaneous variation that is

$$\frac{\omega_{REF}(s)}{\omega_{COM}(s)} = \frac{i_{qREF}(s)}{i_{qCOM}(s)} = \frac{i_{dREF}(s)}{i_{dCOM}(s)} = \frac{1}{\left(\frac{s}{\omega_{ni}}\right)^2 + \frac{2\zeta_i}{\omega_{ni}}s + 1} \qquad (13)$$

ζ_i and ω_{ni} where i = 2, 4 are the desired dominant damping ratio and natural frequency respectively.

3 Extended Luenberger Observer

In this section, the estimation of unknown parameters and state variables are explained by using an observer concept. At the beginning of using this methodology came from studying about "the disturbance observer" that had many pieces of research proposed in the past, such as [13]-[23]. The study found that the disturbance observer has several methodologies, but the distinctive methodology is Extended State Observer (ESO). Due to the robustness against parameter mismatch and signal noise. Also, only observer gains need to be tuned, and the tuning process is not complicated because the gains are determined by the desired observer bandwidth. Refer to the inverse dynamic Equation (6), (7) and (8), the resistance R_s represented by $v_{tq}(=R_s.i_q)$ and load torque T_L are estimated by observer method. In order to apply the methodology, all the system equations are expressed by the state space equation shown as follows.

$$\dot{x}(t) = f(x(t), u(t), t) \qquad (14)$$

$$y(t) = g(x(t), u(t), t) \qquad (15)$$

It is assumed that the time constant of the load torque, and state variable is much larger than of a controller. Thus the derivative of the load torque dT_L/dt and state variable dv_{tq}/dt can be considered as zero. As it a state observer dedicated to the linear system, it was necessary to linearize the considered system around one operating point. The linearization model of PMSM can be written as

$$\dot{x}(t) = \mathbf{A}x(t) + \mathbf{B}u(t) \qquad (16)$$

$$y(t) = \mathbf{C}x(t) \qquad (17)$$

where $x(t) = [i_q\ \omega_m\ v_{tq}\ T_L]^T$, output variables are $y = [i_q\ \omega_m]$ and input variables are $u = [v_q\ i_d]^T$.

$$\mathbf{A} = \begin{bmatrix} 0 & -\frac{\psi_m}{L_q} & -\frac{1}{L_q} & 0 \\ -\frac{p\cdot\psi_m}{J} & -\frac{B}{J} & 0 & -\frac{1}{J} \\ 0 & 0 & 0 & 0 \\ 0 & 0 & 0 & 0 \end{bmatrix} \mathbf{B} = \begin{bmatrix} \frac{1}{L_q} & -p\cdot\omega_{m0} \\ 0 & 0 \\ 0 & 0 \\ 0 & 0 \end{bmatrix} \qquad (18)$$

$$\mathbf{C} = \begin{bmatrix} 1 & 0 & 0 & 0 \\ 0 & 1 & 0 & 0 \end{bmatrix} \qquad (19)$$

The state observer equation by using the luenberger observer is defined as follows.

$$\dot{\hat{x}}(t) = \mathbf{A}\hat{x}(t) + \mathbf{B}u(t) + \mathbf{L}(y(t) - \hat{y}(t)) \qquad (20)$$

$$\hat{y}(t) = \mathbf{C}\hat{x}(t) \qquad (21)$$

$$\dot{\hat{x}}(t) = \mathbf{A}\hat{x}(t) + \mathbf{B}u(t) + \mathbf{LC}(x(t) - \hat{x}(t)) \qquad (22)$$

$$\dot{\hat{x}}(t) = (\mathbf{A} - \mathbf{LC})\hat{x}(t) + \mathbf{B}u(t) + \mathbf{LC}x(t) \qquad (23)$$

The estimated error $e(t) = x(t) - \hat{x}(t)$ is defined:

$$(x(t) - \dot{\hat{x}}(t)) = \mathbf{A}(x(t) - \dot{\hat{x}}(t)) + \mathbf{B}u(t) + \mathbf{LC}(x(t) - \dot{\hat{x}}(t)) \qquad (24)$$

$$\dot{e}(t) = (\mathbf{A} - \mathbf{LC})e(t) \qquad (25)$$

If the matrix gain $\mathbf{L}$ is appropriately designed, the estimated error $e(t) = \hat{x}(t)$- $x(t)$ will tend to zero. It means that the estimated states $\hat{x}(t)$ approach the actual states $x(t)$.

Block diagram for Luenberger observer is shown in Fig. 3. The observability matrix ($\mathbf{Q}_b$) (18), (19) has rank 4. It is full rank, and the system is completely observable. It is realized by choosing the value of the gain matrix $\mathbf{L}$ so that ($\mathbf{A} - \mathbf{LC}$) eigenvalues approach $(-200\ -200\ -33\ -60)^T$. Those values have been tuned experimentally to obtain better performances as possible. For the operating point, at speed (n) = 1500 rpm ω_{m0} = 157.0796 rad/sec, and $i_{d(0)} = 0$, the matrix $\mathbf{L}$ is obtained by (26). For this estimation, even if the system has been linearized around one operating point, it has been experimentally verified that the estimation was converging in the speed range 0-1500 rpm with no change of the value of the matrix $\mathbf{L}$. The closed-loop system pole locations can be arbitrarily placed if and only if the system is controllable.

$$\mathbf{L} = \begin{bmatrix} 260 & -18.811 \\ 395.357 & 230.9174 \\ -423.720 & 0 \\ 0 & -11.088 \end{bmatrix} \tag{26}$$

4 Stability and Control Conclusion

In this section, the stability of the flatness-based control including the extended Luenberger observer is going to be explained. The control conclusion and stability of the flatness-based control was mentioned by [24] that the stability of the control systems was guaranteed. For the stability of the ELO is explained by the design controllers and observers using state-space (or time-domain) methods. For the LTI (Linear Time-Invariant) systems are written as follows.

$$\dot{x}(t) = Ax(t) + Bu(t) \tag{27}$$

$$y(t) = Cx(t) + Du(t) \tag{28}$$

The first step is to analyze whether the open-loop system (without any control) is stable. The eigenvalues of the system matrix, $\mathbf{A}$, (equivalent to the poles of the transfer function) determine the stability. The eigenvalues of the A matrix are the values of s where det($s\mathbf{I}$ - $\mathbf{A}$) = 0. It is important to note that a system must be completely controllable and observable to allow the flexibility to place all the closed-loop system poles arbitrarily. A system is controllable if there exists a control input, $u(t)$, that transfers any state of the system to zero in finite time. It is able be shown that the LTI system (27) is controllable if and only if its controllability matrix, $\mathbf{Q}_c$, has full rank or det($\mathbf{Q}_c$) ≠ 0 (i.e. if rank($\mathbf{Q}_c$) = n where n is the number of states).

$$\mathbf{Q}_c = \left\lfloor \mathbf{B} \,|\, \mathbf{AB} \,|\, \mathbf{A}^2\mathbf{B} \,|\, \ldots \,|\, \mathbf{A}^{n-1}\mathbf{B} \right\rfloor \tag{29}$$

Meanwhile, The system is observable if and only if the observability matrix, $\mathbf{Q}_b$, has full rank or det($\mathbf{Q}_b$) ≠ 0 (i.e. if rank($\mathbf{Q}_b$) = n where n is the number of states).

$$\mathbf{Q}_b = \begin{bmatrix} \mathbf{C} \\ \mathbf{CA} \\ \mathbf{CA}^2 \\ . \\ . \\ . \\ \mathbf{CA}^{n-1} \end{bmatrix} \tag{30}$$

Controllability and observability are dual concepts. A system ($\mathbf{A}$,$\mathbf{B}$) is controllable if and only if a system ($\mathbf{A}'$,$\mathbf{C}$,$\mathbf{B}'$,$\mathbf{D}$) is observable. This fact will be useful when designing an observer. Ackermann's formula can also be employed to place the roots of the observer characteristic equation at the desired locations [25]. Consider the observer gain matrix.

$$\mathbf{L} = [L_1 \quad L_2 \quad \ldots \quad L_n]^T \tag{31}$$

and the desired observer characteristic equation

$$q(\lambda) = \lambda^n + \beta_{n-1}\lambda^{n-1} + \ldots + \beta_1\lambda + \beta_0 \tag{32}$$

The β's are selected to meet given performance specifications for the observer. The observer gain matrix is then computed via

$$\mathbf{L} = q(\mathbf{A})\mathbf{Q}_b^{-1}[0 \quad \ldots \quad 0 \quad 1]^T \tag{33}$$

where $\mathbf{Q}_b$ is the observability matrix and

$$q(\mathbf{A}) = \mathbf{A}^n + \beta_{n-1}\mathbf{A}^{n-1} + \ldots + \beta_1\mathbf{A} + \beta_0\mathbf{I} \tag{34}$$

4 Simulation and Experimental Result

4.1 Laboratory Setup

The main PMSM parameters are presented in Table 1, and the flatness-based controller parameters are defined in Table 2. The laboratory setup showing in Fig. 4 composed of a 6-pole, 1-kW PMSM coupled with a 0.25-kW Separate Excited DC motor that was served as a power supply for a purely resistive load. The stator windings of the PMSM were fed by a 3-kW, 3Φ DC–AC voltage-source inverter (VSI) that was operated at a switching frequency of 10 kHz.

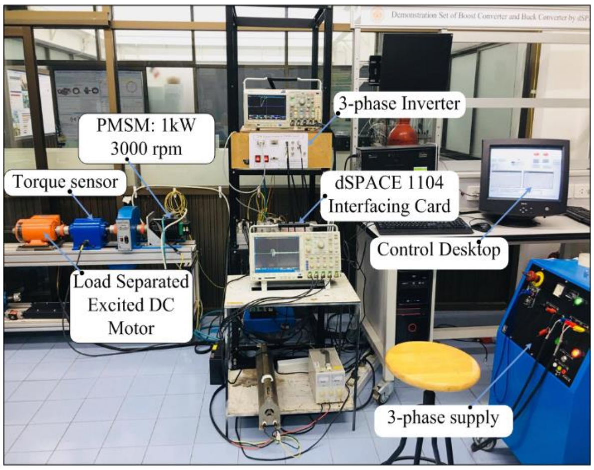

Fig. 4 Test bench setup of the PMSM drive.

Table 1

PMSM/Inverter specification and parameters.

Symbol	Meaning	Value
P_{rated}	Rated Power	1 kW
n_{rated}	Rated Speed	3000 rpm
T_{rated}	Torque Rated	3 Nm
p	Number of Poles pair	
R_s	Resistance (Motor + Inverter)	10.1 Ω
L=L_d=L_q	Stator inductance	35.31 mH
Ψ_m	Magnetic flux	0.2214 Wb
J	Equivalent inertia	0.0022 kg.m^2
B	Viscous friction coefficient	3.5 x 10^{-3} Nm.s/rad
v_{BUS}	DC Bus voltage	530 V
f_s	Switching frequency	10 x 10^3 Hz

Table 2

Speed/current regulation parameters

Symbol	Meaning	Value
ζ_1	Damping ratio 1	1 pu.
ω_{n1}	Natural frequency 1	3200 Rad.s^{-1}
ζ_2	Damping ratio 2	1 pu.
ω_{n2}	Natural frequency 2	320 Rad.s^{-1}
ζ_3	Damping ratio 3	1 pu.
ω_{n3}	Natural frequency 3	32 Rad.s^{-1}
ζ_4	Damping ratio 4	1 pu.
ω_{n4}	Natural frequency 4	32 Rad.s^{-1}
i_{qmax}	The max. quadrature current	+6 A
i_{qmin}	The min. quadrature current	-6 A

The input voltage is obtained through diode rectifier as shown in Fig. 1. The drive system is also equipped with an incremental encoder mounted on the rotor shaft and has a resolution of 4096 lines/revolution.

4.2 Performance of Speed acceleration

Fig. 5 shows the experimental results of speed acceleration response at light load condition (friction losses), n_{COM} 0 – 1500 rpm and i_{dCOM} = 0 A. It is important to mention that the motor speed is able to track accurately the command.

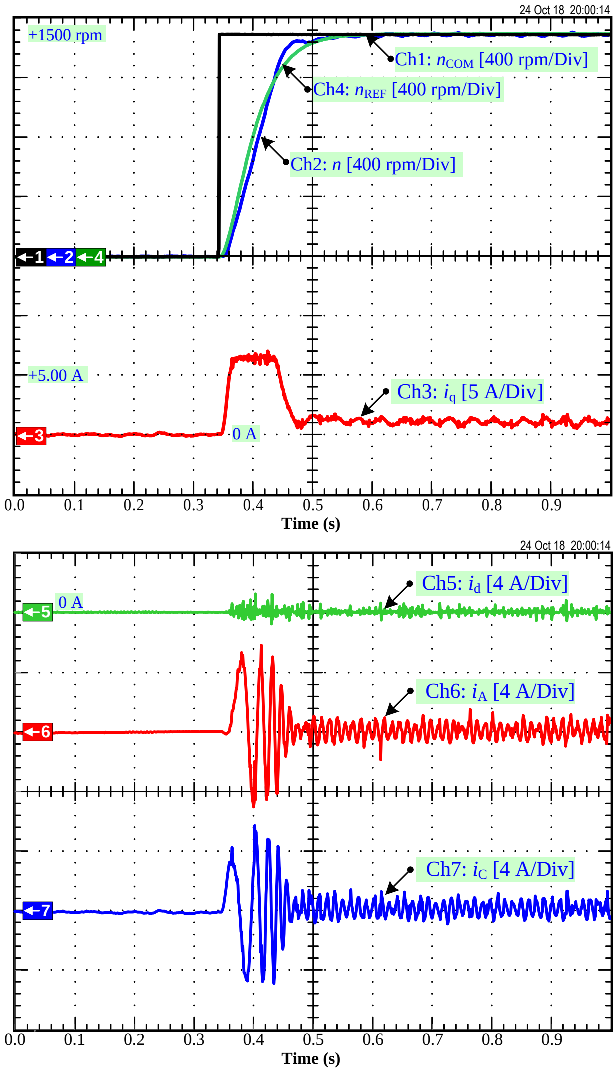

Fig. 5 Experimental results of speed acceleration.

During the acceleration period, the q-axis i_q equals the motor maximum capability (i_{qmax}.= +6 A). This ensures that the PMSM runs up in the shortest time possible, and subsequently the current i_q decreases in order to satisfy the small friction torque.

4.3 Performance of state variables estimation

Fig. 6(a) and 6(b) show the simulation and experimental results respectively of the state variable, T_L estimation. The experimental result is quite corresponding to the simulation results. The results reflect that when the load torque is suddenly applied to PMSM from 0 Nm to 2 Nm, it can be correctly estimated by ELO, and the converging time is less than 0.1 s.

Next, Fig. 7(a) and 7(b) show the simulation and experimental results respectively of state variable, v_{tq}=(R_s.i_q) estimation. The experimental result is coincident to the simulation result. In the figure illustrates that v_{tq} can be precisely estimated by the proposed observer.

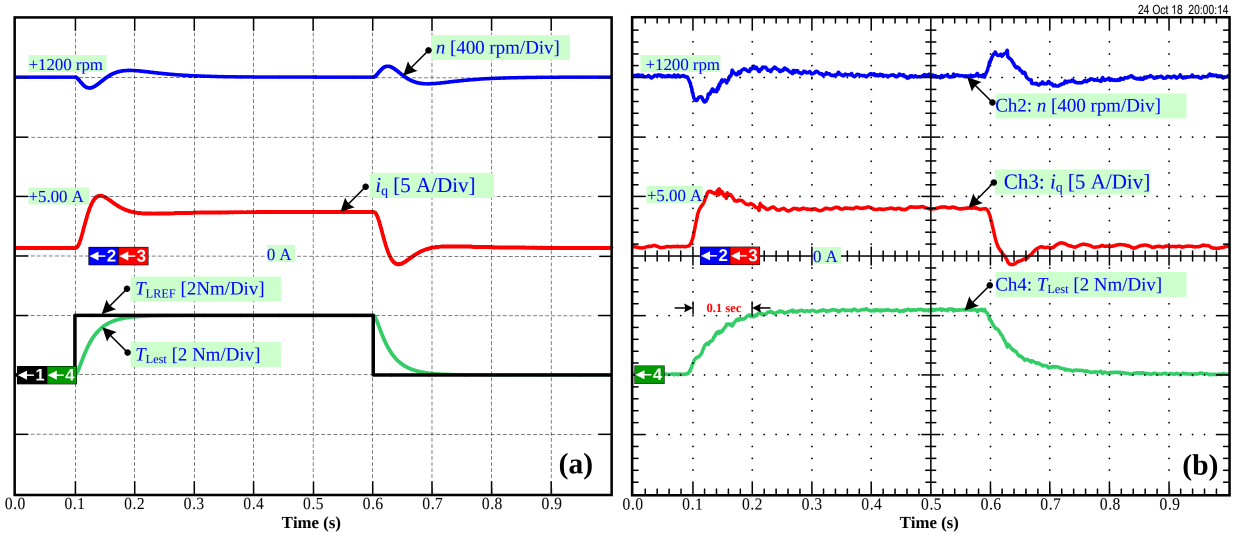

Fig. 6 Simulation and experimental results of TL estimation: (a) Simulation and (b) Experimental.

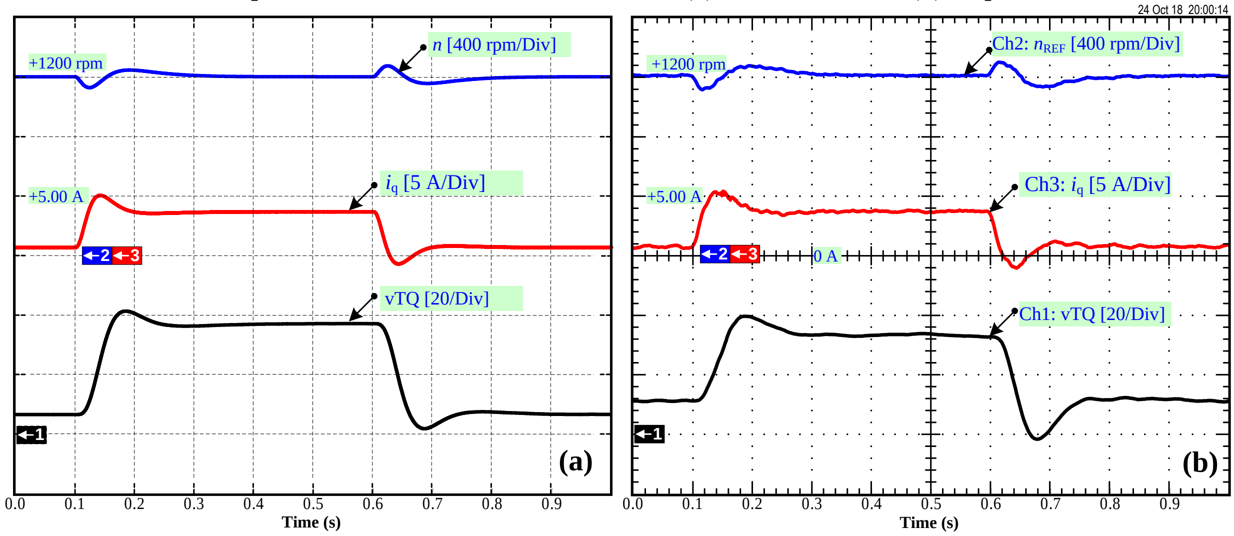

Fig. 7 Simulation and experimental responses of v_{tq} estimation: (a) Simulation and (b) Experimental.

4.4 Speed Reversal of flatness-based controller

The experimental results of speed reversal responses of the system demonstrate in Fig. 8, where the motor is forced to reverse its direction. The system operates in a regenerative mode until the speed of the rotor will become positive; and thereafter, the system changes to motoring mode until the rotor speed reaches reference value. The experimental results reflect that the speed of PMSM can efficiently be controlled by flatness-based control. During steady-state region, the speed measurement is able to almost 100% track the speed reference and the speed command, and *q*-axis current is restrained without exceeding the current limitation (+6 Ampere).

4.3 Performance of disturbance rejection

To guarantee the stability of the control system, in this section is going to illustrate the response of the whole systems shown in Fig. 9 that including Ch1: speed measurement *n*, Ch2: *q*-axis current i_q, Ch3: *d*-axis current i_d, Ch4: T_{Lest}, Ch5: v_{tq}, Ch6: phase current i_a, Ch7: phase current i_c, and the trajectories of the transient stator current vector. The results reflect that the stability of flatness-based control and ELO is appropriately designed. These results show that the ELO has better disturbance rejection ability. Moreover, the performance of the proposed control is improved because the performance of the control system depends on these parameters of the machine.

4.5 Comparison between Flatness-based and PI Controller

PI controller for the PMSM drive is going to describe briefly in this section because it has mentioned in the introduction section. Fig. 10 shows the block diagram of the closed-loop transfer function of the current control. K_{pi} and K_{ii} parameters are determined according to (35), (36). This approach explained by [26].

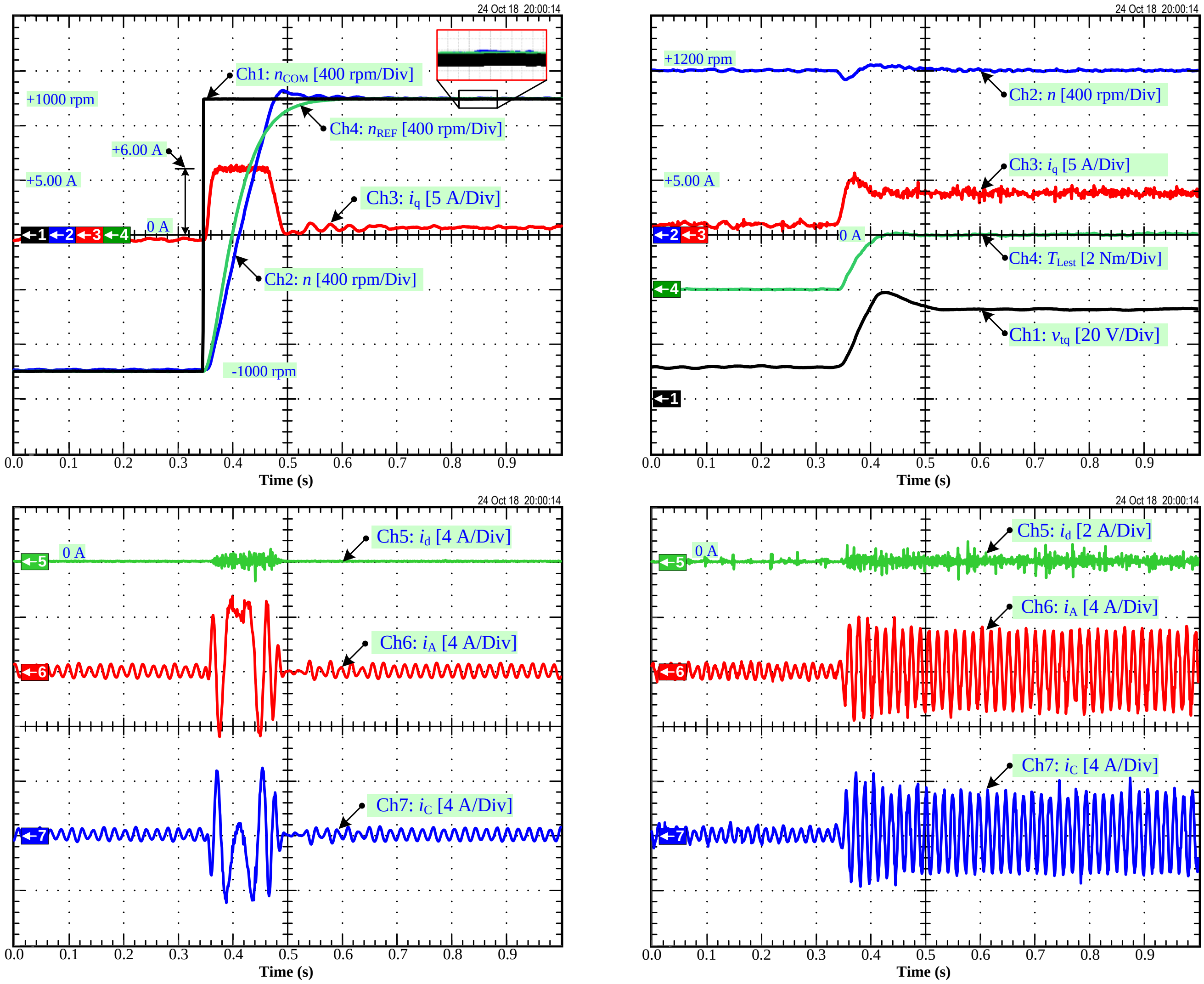

Fig. 8 Experimental results of speed reversal.

τ_s was obtained by checking the step response and pick the time when step response reaches 63.2 % of the steady-state value.

$$K_{pi} = 2\zeta_i R_s \tau_s \omega_{ni} - R_s \tag{35}$$

$$K_{pi} = R_s \tau_s \omega_{ni}^2 \tag{36}$$

where $\zeta_i = 1$ and $\omega_{ni} = 286.0379$ rad/sec.

Next, the closed-loop transfer function between ω_{REF} and ω_m is represented by a block diagram, as shown in Fig 11. The lag compensator (or PI controller) expressed by (37) is achieved by sisotool (plant)

$$G_c = \frac{0.12(s+70)}{(s)} \tag{37}$$

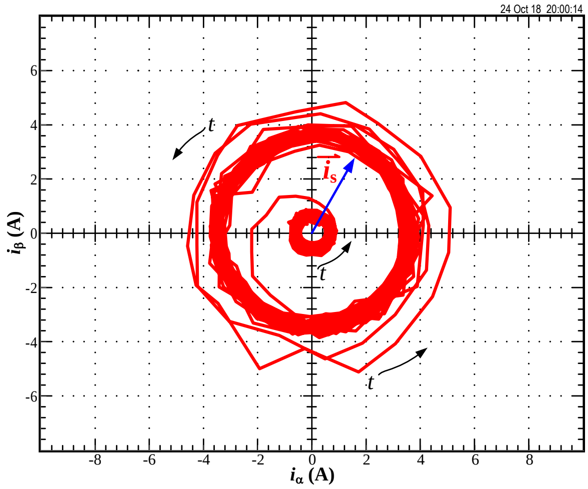

Fig. 9 Experimental results of disturbance rejection.

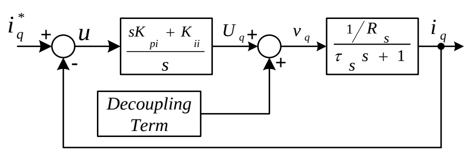

Fig. 10 Closed-loop current control transfer function.

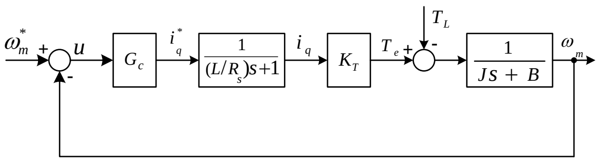

Fig. 11 Closed-loop speed control transfer function.

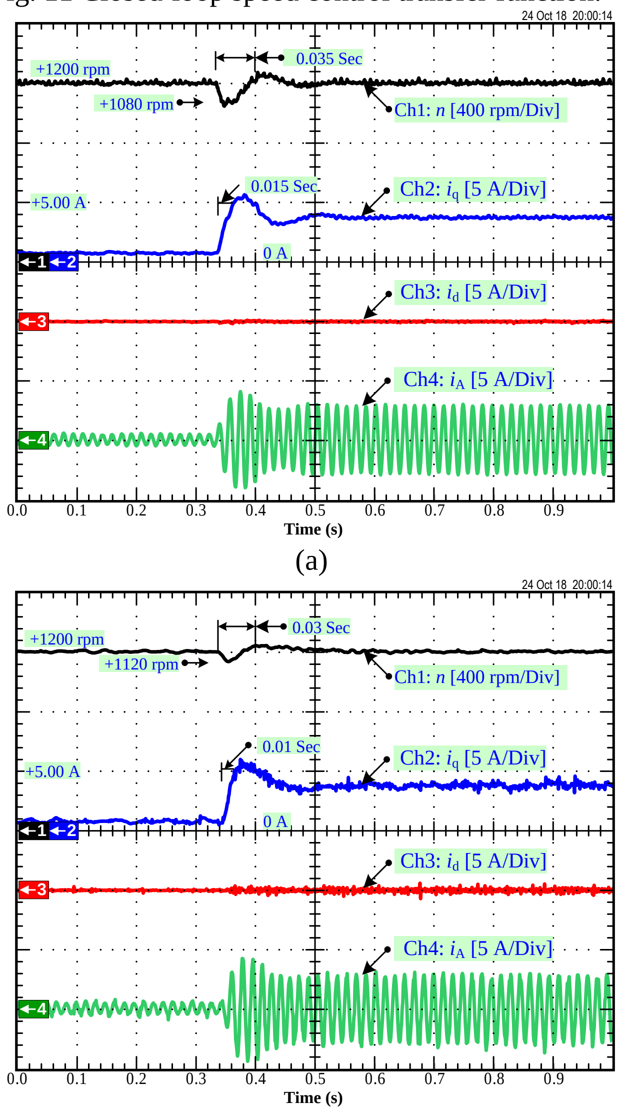

(a)

(b)

Fig. 12 Experimental results of comparison between PI control and flatness-based control.

Fig. 12(a) and 12(b) show the experimental result of the PI control and the flatness-based control respectively. In the oscilloscope illustrates, Ch1: is the speed measurement n, Ch2: is the q-axis current i_q, Ch3: is the d-axis current i_d, and Ch4: is the phase A current i_A. The results reflect that the flatness-based control speed fluctuation is approximately 80 rpm while that with PI controller is 120 rpm, and the recovery time of speed with flatness-based control is approximately 0.03 sec while that with PI control is 0.035 sec. Additionally, the transient time response of flatness-based control is approximately 0.01 sec while that with the PI control is 0.015 sec. This demonstrates that the flatness-based control has better dynamic performance than a PI control.

4 Conclusion

This paper has presented the state variables estimation using the extended Luenberger observer to improve the performance of flatness-based control for PMSM Drive. It turns out that the extended Luenberger observer has better disturbance rejection ability. Additionally, the performance of the proposed control is improved because the performance of the controller depends on these parameters of the machine. A test bench has been developed using a PMSM drives to practically illustrate the benefits of the proposed controller. The experimental results have shown the ability of the proposed approach to reject the effect of the uncertainty disturbance torque and a resistance in series with an inductance and the switching as well as conduction losses in semiconductor switching devices of inverters. Thereby, the proposed control design provides practitioners with an alternative and effective method to build a robust nonlinear controller.

References:

[1] Q. Liu and K. Hameyer, "High-Performance Adaptive Torque Control for an IPMSM With Real-Time MTPA Operation," *IEEE Trans. Energy Convers.*, Vol. 32, No. 2, 2017, pp. 571-581.

[2] F. F. M. El-Sousy, "Intelligent Optimal Recurrent Wavelet Elman Neural Network Control System for Permanent-Magnet Synchronous Motor Servo Drive," *IEEE Trans. Ind. Informatics*, Vol. 9, No. 4, 2013, pp. 1986-2003.

[3] Y. S. Choi, H. H. Choi, and J. W. Jung, "Feedback Linearization Direct Torque Control With Reduced Torque and Flux Ripples for IPMSM Drives," *IEEE Trans. Power Electronics*, Vol. 31, No. 5, 2016, pp. 3728-3737.

[4] W. H. Chen, J. Yang, L. Guo and S. Li, "Disturbance-Observer-Based Control and Related Methods—An Overview," *IEEE Trans. Ind. Electron.*, Vol. 63, No. 2, 2016, pp. 1083-1095.

[5] W. Xie et al., "Finite-Control-Set Model Predictive Torque Control With a Deadbeat Solution for PMSM Drives," *IEEE Trans. Ind. Electron.*, Vol. 62, No. 9, 2015, pp. 5402-5410.

[6] Y. C. Chang, C. H. Chen, Z. C. Zhu and Y. W. Huang, "Speed Control of the Surface-Mounted Permanent-Magnet Synchronous Motor Based on Takagi–Sugeno Fuzzy Models," *IEEE Trans. Power Electron.*, Vol. 31, No. 9, 2016, pp. 6504-6510.

[7] R. Cai, R. Zheng, M. Liu and M. Li, "Robust Control of PMSM Using Geometric Model Reduction and μ-synthesis," *IEEE Trans. Ind. Electron.*, Vol. PP, No. 99, 2018, pp. 1-1.

[8] H. Li, J. Wang, H. K. Lam, Q. Zhou and H. Du, "Adaptive Sliding Mode Control for Interval Type-2 Fuzzy Systems," IEEE Trans. Syst., Man, Cybern., Syst., Vol. 46, No. 12, 2016, pp. 1654-1663.

[9] P. Thounthong et al., “Model based control of permanent magnet AC servo motor drives,” in *Proc. Electrical Machines and Systems (ICEMS)*, 2016, pp. 1-6.

[10] H. Sira-Ramírez, J. Linares-Flores, C. García-Rodríguez and M. A. Contreras-Ordaz, "On the Control of the Permanent Magnet Synchronous Motor: An Active Disturbance Rejection Control Approach," *IEEE Trans. Control Syst. Technol.*, Vol. 22, No. 5, 2014, pp. 2056-2063.

[11] M. Yang, X. Lang, J. Long and D. Xu, "Flux Immunity Robust Predictive Current Control With Incremental Model and Extended State Observer for PMSM Drive," ” *IEEE Trans. Power Electron.*, Vol. 32, No. 12, 2017, pp. 9267-9279.

[12] P. Pillay and R. Krishnan, "Control characteristics and speed controller design for a high performance permanent magnet synchronous motor drive," *IEEE Trans. Power Electron.*, Vol. 5, No. 2, 1990, pp. 151-159.

[13] L. Wang, J. Jatskevich and H. W. Dommel, "Re-examination of Synchronous Machine Modeling Techniques for Electromagnetic Transient Simulations," *IEEE Trans. Power Syst.*, Vol. 22, No. 3, 2007, pp. 1221-1230.

[14] N. Matsui, T. Makino and H. Satoh, "Autocompensation of torque ripple of direct drive motor by torque observer," *IEEE Trans. Ind. Appl.*, Vol. 29, No. 1, 1993, pp. 187-194.

[15] J. Solsona, M. I. Valla and C. Muravchik, "Nonlinear control of a permanent magnet synchronous motor with disturbance torque estimation," *IEEE Trans. Energy Convers.*, Vol. 15, No. 2, 2000, pp. 163-168.

[16] Y. A. R. I. Mohamed, "Design and Implementation of a Robust Current-Control Scheme for a PMSM Vector Drive With a Simple Adaptive Disturbance Observer," *IEEE Trans. Ind. Electron.*, Vol. 54, No. 4, 2007, pp. 1981-1988.

[17] Y. Zhang, C. M. Akujuobi, W. H. Ali, C. L. Tolliver and L. S. Shieh, "Load Disturbance Resistance Speed Controller Design for PMSM," *IEEE Trans. Ind. Electron.*, Vol. 53, No. 4, 2006, pp. 1198-1208.

[18] W. Deng, C. Xia, Y. Yan, Q. Geng and T. Shi, "Online Multiparameter Identification of Surface-Mounted PMSM Considering Inverter Disturbance Voltage," *IEEE Trans. Energy Convers.*, Vol. 32, No. 1, 2017, pp. 202-212.

[19] S. Diao, D. Diallo, Z. Makni, C. Marchand and J. F. Bisson, "A Differential Algebraic Estimator for Sensorless Permanent-Magnet Synchronous Machine Drive," *IEEE Trans. Energy Convers.*, Vol. 30, No. 1, 2015, pp. 82-89.

[20] F. Tinazzi and M. Zigliotto, "Torque Estimation in High-Efficency IPM Synchronous Motor Drives," *IEEE Trans. Energy Convers.*, Vol. 30, No. 3, 2015, pp. 983-990.

[21] Y. Sangsefidi, S. Ziaeinejad, A. Mehrizi-Sani, H. Pairodin-Nabi and A. Shoulaie, "Estimation of Stator Resistance in Direct Torque Control Synchronous Motor Drives," *IEEE Trans. Energy Convers.*, Vol. 30, No. 2, 2015, pp. 626-634.

[22] G. Wang et al., "Enhanced Position Observer Using Second-Order Generalized Integrator for Sensorless Interior Permanent Magnet Synchronous Motor Drives," *IEEE Trans. Energy Convers.*, Vol. 29, No. 2, 2014, pp. 486-495.

[23] H. Renaudineau, J. P. Martin, B. Nahid-Mobarakeh and S. Pierfederici, "DC–DC Converters Dynamic Modeling With State Observer-Based Parameter Estimation," *IEEE Trans. Power Electron.*, Vol. 30, No. 6, 2015, pp. 3356-3363.

[24] Thounthong, P., S. Pierfederici, et al., "Analysis of Differential Flatness-Based Control for a Fuel Cell Hybrid Power Source," *IEEE Trans. Energy Convers.*, Vol. 25, No. 2, 2010, pp. 909-920.

[25] Dorf, R. C. and R. H. Bishop, *Modern control systems, 12th ed.*, Publishing Pearson, 2011, pp. 847–850.

[26] Sheng-Ming Yang and Kuang-Wei Lin, "Automatic Control Loop Tuning for Permanent-Magnet AC Servo Motor Drives," *IEEE Trans. ind. Electron.*, Vol. 63, Vo. 3, 2016, pp. 1499-1506.